



# Magnesium oxide-poly( $\epsilon$ -caprolactone)-chitosan-based composite nanofiber for tissue engineering applications

Nava P. Rijal<sup>a,d,1</sup>, Udhab Adhikari<sup>b,d,1</sup>, Shalil Khanal<sup>c,d</sup>, Devdas Pai<sup>b,d</sup>, Jagannathan Sankar<sup>b,d</sup>, Narayan Bhattarai<sup>a,d,\*</sup>

<sup>a</sup> Department of Chemical, Biological, and Bioengineering, North Carolina A&T State University, Greensboro, NC 27411, USA

<sup>b</sup> Department of Mechanical Engineering, North Carolina A&T State University, Greensboro, NC 27411, USA

<sup>c</sup> Department of Energy and Environmental Systems, North Carolina A&T State University, Greensboro, NC 27411, USA

<sup>d</sup> NSF-ERC for Revolutionizing Metallic Biomaterials, North Carolina A&T State University, Greensboro, NC 27411, USA

## ARTICLE INFO

### Keywords:

Nanofiber  
Polycaprolactone  
Magnesium  
Chitosan  
3T3 fibroblast  
Tissue engineering

## ABSTRACT

The ability to produce composite nanofibers of inorganic particles and synthetic polymers represents a significant advancement in the development of composite materials for potential biomedical applications. In this study, composite nanofibers of magnesium oxide (MgO), poly( $\epsilon$ -caprolactone) (PCL) and chitosan (CS) with diameters in the range of 0.7–1.3  $\mu\text{m}$  were fabricated by electrospinning their blend solutions in trifluoroethanol and water. To support the potential use of these nanofibrous membranes for biomedical applications their physicochemical properties such as morphology, mechanical strength, and integrity in aqueous medium, were studied. Cellular compatibility was determined using cell viability assays and microscopy imaging, with the results showing that the nanofibrous membranes support 3T3 cell viability and attachments. The new composite nanofibrous membranes developed in this study have the ability to mimic the physical structure and function of tissue extracellular matrix (ECM) and thus have potential for many tissue engineering applications.

## 1. Introduction

Engineered composite nanofibers have shown great potential in different biomedical applications including but not limited to drug delivery, wound healing, tissue engineering, implant coatings etc. [1–4]. Nanofibers having high surface-area-to-volume ratio produce scaffolds with unique physicochemical properties that can closely resemble the properties of extracellular matrix (ECM) components found in natural tissues [5]. For the last few years, electrospinning has been recognized as an efficient and reliable technique to create nanofibers [6–9]. Electrospinning is a simple and versatile technique that allows the engineering of scaffolds with micro-to-nanoscale topography and with porosity that can be tuned to match the tissue ECM [10].

Composite nanofibers derived from natural and/or synthetic biopolymers and ceramic particulates are gaining popularity in biomedical applications because they capitalize on the favorable biological properties of the natural polymer and the ceramic, and superior mechanical properties of the synthetic polymer [11]. However, effective synthesis of well-blended composite fibers remains a great challenge due to the poor miscibility between polymers and ceramic particles at the

molecular level. As a result of phase separation, poorly blended composite nanofibers exhibit weak mechanical strength and uncontrollable material properties [11,12].

A large body of published work in the area of chitosan (CS) and polycaprolactone (PCL) blends demonstrates the growing interest in CS-PCL composite fibers for biomedical applications where mechanical strength, biocompatibility and stability of nanofibers *in vitro* and *in vivo* are important [13,14]. CS, a polysaccharide derived from the exoskeletons of crustaceans shares structural similarity with glycoasamine glycan (GAG), a major component of tissue ECM. Therefore, the nanostructured morphology of the CS-PCL composite fibers better represents the ECM of tissues and serve as an excellent framework for cell adhesion, proliferation, and differentiation. Due to chitosan's versatile characteristics, it makes an excellent choice for controlled release formulations, including non-viral vectors for DNA-gene and drug delivery, imaging, wound healing, and smart implant coating applications [15–17]. The complementary polymer, PCL, an aliphatic synthetic polymer, is a widely-used material in tissue engineering. PCL is biocompatible and has mechanical properties superior to natural polymers [18]. On the other hand, PCL lacks desirable cell affinity, primarily due

\* Corresponding author.

E-mail address: [nbhattar@ncat.edu](mailto:nbhattar@ncat.edu) (N. Bhattarai).

<sup>1</sup> Authors have equal contributions.

to its hydrophobicity and lack of cell recognition sites. This results in decreased cell proliferation and differentiation [18]. Most natural and synthetic polyblends such as gelatin/PCL and collagen/PCL require chemical crosslinking agents to retain their structure and maintain mechanical properties. Unfortunately, the crosslinking agents simultaneously yield toxic residues [18]. However, appropriately constructed PCL-CS/MgO composites offer the benefit of integrating the favorable biological properties of CS with the favorable mechanical properties of PCL without requiring chemical crosslinking to retain their structure and desirable mechanical properties. MgO, a ceramic, is an inorganic salt of magnesium that releases  $Mg^{++}$  ions.  $Mg^{++}$  is the second most abundant intracellular cation, and is important to human metabolism. Recent studies have shown that the divalent cations such as  $Mg^{++}$  play a crucial role in providing effective function of nerve tissue, and in repairing nerve damage as well as in bone remodeling and skeletal development [19–21]. The choice of Mg was further motivated by its excellent biocompatibility, biodegradation into non-toxic products and its proven role in different processes such as cellular respiration, protein synthesis, membrane integrity, ATPase function and oxidative phosphorylation [22–24].

Among a large number of inorganic particulates used to design composite nanofibers, there has been a growing interest in magnesium oxide (MgO)-based composite materials because of its decontamination potential for catalytic detoxification of toxic chemicals as well as protection from UV light [25–28]. These composites have great potential to protect against chemical warfare stimulants [25,27,28]. Although there has been some success in producing MgO-based composite nanofibers, very limited studies have been done on MgO-incorporated nanofiber membrane as potential scaffold material for tissue engineering applications [26,29]. In this research, therefore, we seek to improve the miscibility of MgO in poly ( $\epsilon$ -caprolactone) (PCL) as well as poly ( $\epsilon$ -caprolactone)-chitosan (PCL-CS) solution systems, and to study the mechanical and biological properties of the composite nanofiber electrospun from the solutions.

We fabricated nanofiber membranes of PCL-CS/MgO of different compositions by electrospinning the blend solutions of PCL and MgO in trifluoroethanol, and CS in water. Physicochemical properties, such as morphology, mechanical strength, and integrity in aqueous medium as well as cellular compatibility of the nanofibrous membrane were determined.

## 2. Materials and methods

### 2.1. Materials

Chitosan (MW 2.5 k; Lot No. HL130109G) was purchased from Creative PEGWorks Inc. (Chapel Hill, NC). 2,2,2-Trifluoroethanol (TFE) was obtained from Alfa Aesar (Ward Hill, MA). PCL (Mn 70–90 kDa), and MgO (nanopowder, < 50 nm particle size) were purchased from Sigma Aldrich. Stainless steel dispensing needle (21 gauge and 3.81 cm long, product number 75165A757), fluorinated ethylene propylene tubing (0.32 cm inner diameter) and Luer lock syringe needle fittings were obtained from McMaster-Carr (Atlanta, GA). Luer-lock syringes (catalog number: 14-829-45) was obtained from Fisher Scientific (Pittsburgh, PA).

### 2.2. PCL/MgO and PCL-CS/MgO solution preparation

PCL and CS were dissolved in separate beakers at a concentration of 10% (w/w) in TFE and DI water respectively. PCL/MgO solutions were created by mixing PCL and MgO in different ratios (Table 1). Subsequently, a PCL-CS/MgO solution was created by mixing CS solution drop-wise to the solution of PCL and MgO. The solution mixtures were vortexed manually until each solution reached a homogeneous blend

**Table 1**  
Fiber sample compositions.

Set A				
Sample	Concentration of PCL (wt%)	Relative amount of PCL	Relative amount of MgO	
PCL	10	100	0	
PCL/MgO	10	90	10	
PCL/MgO	10	75	25	
PCL/MgO	10	50	50	
Set B				
Sample	Concentration of CS (wt%)	Concentration of PCL (wt%)	Relative amount of PCL-CS	Relative amount of MgO
PCL-CS	10	10	100	0
PCL-CS/MgO	10	10	90	10
PCL-CS/MgO	10	10	75	25
PCL-CS/MgO	10	10	50	50

ready for electrospinning. Weight ratio of PCL/CS was maintained at 80/20 for all the CS based blend solutions.

### 2.3. Electrospinning of PCL/MgO and PCL-CS/MgO nanofibers

A previously prepared polymer solution of PCL/MgO and PCL-CS/MgO was individually fed into the syringe of 10 mL and then placed into a syringe pump (Model 78-01001, Fisher Scientific, Pittsburgh, PA, USA). The syringe pump was set to a flow rate of 2.5 mL/h. The syringe tip was positioned ~7 cm from a fiber collecting drum at an angle of ~30° to the horizontal. A 25–27 kV high voltage power supply (Model CZE100PN30, Spellman High Voltage Electronics Corporation, Hauppauge, NY, USA) was used to charge the solution. The positive lead from the high voltage power supply was fixed to a 21-gauge hypodermic needle. The fibers formed were deposited onto an aluminum sheet wrapped over a rotating grounded collector.

### 2.4. Nanofiber morphology study

The surface morphology of nanofiber membranes was analyzed by SEM (Hitachi SU8000, Tokyo, Japan). Prior to imaging, a small section of the fibers was sputter coated with gold in a Polaron SEM coating system for 90 s at 15 mA. Images of the samples were taken at an accelerating voltage of 10 kV and 5  $\mu$ A current. The diameter of these electrospun fibers was determined through SEM images with the use of ImageJ Pro Plus 6.0 software (NIH, USA). Three SEM images from different location of each composition were utilized. Twenty different nanofibers were randomly chosen in each SEM image to measure the diameter in pixels. The number of pixels was converted into  $\mu$ m using the scale factor. Finally, the average diameter of the nanofibers was calculated based on the converted ImageJ data.

The core-shell structure of the electrospun PCL/MgO composite nanofibers was examined in a Tecnai G2 Twin transmission electron microscope (TEM) at 200 kV. The samples for TEM were prepared by directly depositing the as-spun nanofibers onto a copper grid.

Stability and degradation of nanofiber membranes were also studied through SEM images. Sterilized nanofiber membrane of PCL, PCL/CS and PCL-CS/MgO (30  $\times$  30 mm) immersed in 40 mL of 1X Phosphate Buffer Saline (PBS) solution were incubated for 3 weeks in a Shaking Incubator (Dubnoff Shakebath-2876, Thermo Fisher Scientific, Fair Lawn, NJ, USA) at 37 °C and 50 rpm. Nanofibers after incubation were removed from the PBS solution, rinsed with DI water and lyophilized.

Morphological changes on these samples were studied under SEM.

### 2.5. Mechanical testing

Mechanical properties of the fiber were determined with a universal testing machine (Instron 5542) with a 500 N load cell at a displacement rate of 4 mm/min. A custom-designed specimen holder was used to test the fiber strength. A paper template of (38 mm × 25 mm) with an opening of (6 mm × 12 mm) was prepared as described in the literature [18,26] in order to avoid any damage to the fibers during handling and to maintain uniformity in loading conditions. Width, thickness and initial length of the fiber mats were calculated by digital micrometer. Fiber samples were strained to breaking, and Young's modulus and ultimate tensile strength were calculated from the stress–strain curves.

### 2.6. X-ray diffraction

A Bruker AXS D8 Discover X-ray diffractometer with Cu-K $\alpha$  radiation was used to examine the crystallography and phases of the nanofiber membranes synthesized. The X-ray diffraction patterns were recorded in locked-coupled scan mode with a scanning range (diffraction angle, 2 $\theta$ ) set between 10° and 80°. The instrument was operated in the continuous mode, in increments of 0.0146°. All experiments were performed at room temperature.

### 2.7. FTIR analysis

Fourier transform infrared spectroscopy (FTIR) was used to analyze the bonding between PCL and CS in the fiber. FTIR spectra were recorded using Varian 670 FT-IR Spectrophotometer (Varian, Inc., Palo Alto, CA, USA). The spectra were collected from 400 to 4000 cm<sup>-1</sup> with a resolution of 4 cm<sup>-1</sup>.

### 2.8. Cell seeding

Nanofiber samples were attached to a circular coverslip using a biocompatible silicone-based elastomeric gel [18]. The membrane was first wrapped around a circular coverslip and glued carefully at the back of the coverslip. Front side with the porous structure was made available for cell attachment and infiltration. The nanofiber samples were sterilized in 24-well plates by incubating in 95% ethanol for 30 min under a sterile fume hood. After 30 min, samples were rinsed with sterile DI water (twice) and 1X DPBS prior to cell seeding. 1 mL of the growth medium Dulbecco's modified Eagle's medium (DMEM) (Life Technologies, Grand Island, NY) supplemented with 10% fetal bovine serum (FBS) and 1% antibiotics (10,000 units/mL of penicillin and 10,000  $\mu$ g/mL of streptomycin) were added to each well plate and incubated for 3 h. NIH/3T3 cells (a mouse fibroblast cell line) were purchased from the American Tissue Type Culture Collection (Manassas, VA). The cells were cultured in a 75 cm<sup>2</sup> culture flask and maintained in a tissue culture incubator at 37 °C and 5% CO<sub>2</sub> atmosphere. The culture medium was replaced every 2 days. After reaching about 90% confluence, the cells were detached by 0.025% trypsin and 0.01% EDTA in PBS solution and transferred to a centrifuge tube containing the culture medium. After centrifuging, the cells were re-suspended in fresh culture medium and counted using a hemocytometer before seeding to nanofiber samples. A 95  $\mu$ L aliquot of medium containing cells (~50,000) was seeded on nanofiber samples (n = 3) and grown in a humidified incubator (37 °C, 5% CO<sub>2</sub>) for 1, 2 and 3 days, respectively.

### 2.9. Alamar Blue assay and study of pH change

The Alamar Blue (AB) colorimetric assay (Life Technologies, Grand Island, NY) was used to analyze the cell attachment and cell

cytotoxicity of 3T3 fibroblast cells grown on composite nanofiber samples on coverslips and, as a control, on plain glass coverslips. After 1 and 3 days of culture, the culture plates were removed from the incubator, media was removed from the sample and washed twice with DPBS and incubated with 1 ml of 10 % (v/v) AB containing DMEM with 10% FBS for 2 h. After incubation, 400- $\mu$ L sample of the assay solution was transferred to an opaque 96-well culture plate for fluorescent measurements on a SPECTRAMax GEMINI XPS microplate spectrofluorometer (Molecular Devices, Sunnyvale, CA) at  $\lambda_{ex}$  530 nm,  $\lambda_{em}$  590 nm. The relative fluorescent units were converted to a percent of the average values for cells in control wells.

Initial pH of the cell culture media (DMEM supplemented with 10% FBS, 1% antibiotics) was recorded using a Fisher Scientific™ Accumet™ AE150 pH Benchtop meter. Similarly, before the AB assay, pH of cell culture media was determined for 1, 2 and 3 days respectively.

### 2.10. Cell fixation and cell attachment

After the cell cytotoxicity assay, samples with cells were fixed and cellular morphology was examined with SEM. Cells were washed with DPBS (twice) and fixed with 4% glutaraldehyde for 30 min. After fixing, samples were briefly rinsed with DI water (twice) and dehydrated by sequential incubations in 50, 75, and 100% ethanol at room temperature. The sequential wash between different percent of ethanol was carried out at 10 min-intervals. The samples were left to dry in the sterile fume hood for 24 h and were imaged using SEM.

### 2.11. Statistical analysis

Statistical analysis was performed using a one-way analysis of variance (ANOVA). p-values less than .05 were considered statistically significant, and the Tukey test method was conducted for pairwise comparisons. SPSS Statistics 17.0 software was used to conduct the statistical analysis.

## 3. Results

### 3.1. Nanofiber morphology

The surface morphology of as-synthesized nanofibers of PCL, PCL/MgO and PCL-CS/MgO is shown in Fig. 1. Fig. 1A shows the morphology of pure PCL nanofibers whereas images of Fig. 1B–D show PCL nanofiber with increasing concentration of MgO. Similarly, Fig. 1E shows structure of polyblended PCL–CS fiber and Fig. 1F–H represents the morphology of PCL-CS nanofibers with increasing MgO concentration. The average diameters of PCL, PCL/MgO (90/10), PCL/MgO (75/25) and PCL/MgO (50/50) were found to be 1.30, 1.10, 1.00 and 0.97  $\mu$ m, respectively (n = 20). There was a statistically significant difference (p = .0437) in fiber diameter between PCL and PCL/MgO (50/50). Similarly, the average diameters of PCL/CS, PCL-CS/MgO (90/10), PCL-CS/MgO (75/25) and PCL-CS/MgO (50/50) were 0.70, 0.90, 0.93 and 0.95  $\mu$ m respectively (n = 20). There was a significant difference (p = .00627 and .02386) in fiber diameter of PCL with PCL-CS/MgO (90/10) and PCL-CS/MgO (50/50) fiber respectively.

PCL fibers were bead-free, had a smooth surface, and were oriented in a single direction. PCL/MgO fiber, however, showed small protrusions and had a rough fiber structure. The distinct morphology of nanofibers produced from the solution of PCL alone is attributed to solution conductivity and solution viscosity [30]. In Fig. 1E, random orientation of fibers can be seen as compared to PCL fibers. Furthermore, addition of CS (Fig. 1H) resulted in the formation of small fibrous networks (50–70 nm in diameter) between major nanofibers.

The surface morphology and particle distribution was further observed by using Transmission Electron Microscopy. Fig. 2A, B shows TEM images of the electrospun PCL nanofibers with and without MgO

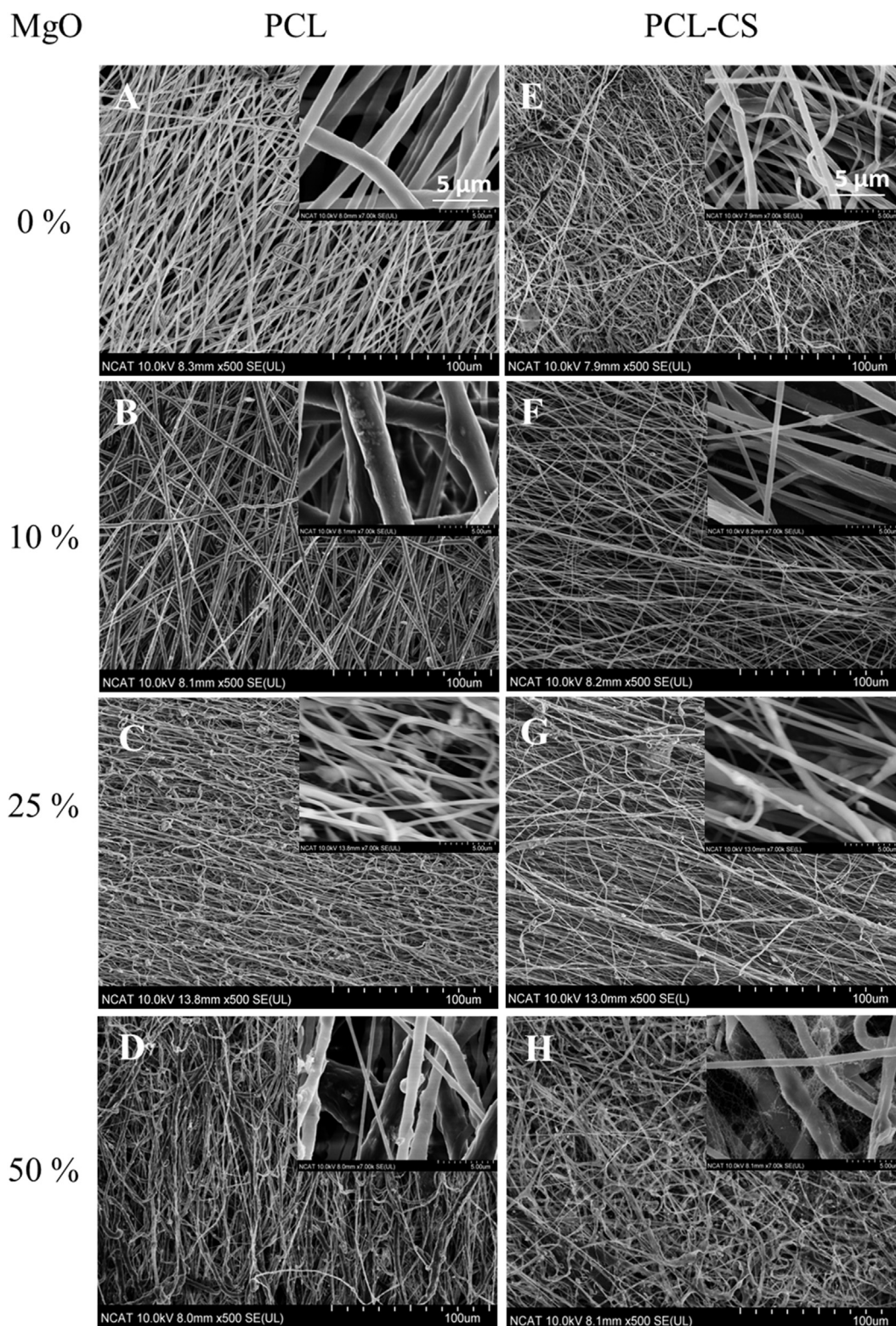


Fig. 1. SEM images showing the morphology of nanofiber membranes. Images A to H represent PCL, PCL/MgO (90/10), PCL/MgO (75/25), PCL/MgO (50/50), PCL/CS, PCL-CS/MgO (90/10), PCL-CS/MgO (75/25) and PCL-CS/MgO (50/50) respectively. Insets are the higher magnification images of the corresponding SEM images of the nanofiber.

nanoparticles ( $< 50$  nm). The array of MgO nanoparticles are seen to be encapsulated in the PCL nanofibers.

Next, nanofiber membranes were studied for their stability. Samples were immersed in PBS (1X) for 3 weeks and these fiber membranes retained their dimensional stability as well as fibrous structure throughout the test period which is confirmed by SEM images in Fig. 3.

### 3.2. Mechanical properties of the fiber

Mechanical properties of nanofibers were assessed by tensile testing. Results of ultimate tensile strength (UTS) and Young's Modulus (YM) are shown in Figs. 4 and 5. The Young's Modulus was determined using Hooke's law from the slope of the linear portion of the stress-strain

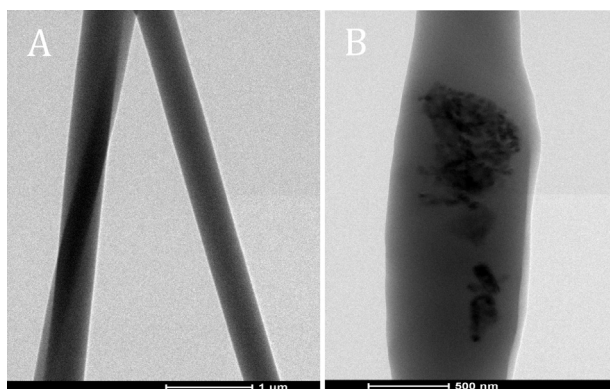


Fig. 2. TEM images showing the morphology of nanofiber membrane. Images A and B represent PCL and PCL/MgO respectively.

curve, whereas the UTS was determined as the highest stress that a nanofiber sample could bear without breaking [18,29]. The ultimate tensile strength for PCL nanofiber was found to be 2.8 MPa and these values were 1.9, 2.2 and 2.1 MPa for PCL nanofibers which contained 10, 25 and 50% MgO respectively. Similarly, the ultimate tensile strength for PCL-CS nanofiber was found to be 3.3 MPa. PCL-CS nanofiber with 10, 25 and 50% MgO had 2.3, 2.6 and 2.5 MPa UTS respectively. There was a significant ( $p = .02083$ ) decrease in UTS when 10% MgO was added to PCL. However, there was no significant difference in UTS when the concentration of MgO was further increased from 10% to 25% and 50%. There was no significant difference in UTS when CS was added to PCL but a significant ( $p = .0067$ ) decrease in UTS was observed when 10% MgO was added to PCL-CS. Similar to PCL nanofibers, there was no significant difference in UTS of PCL-CS nanofibers when MgO concentration was increased further from 10%.

Furthermore, the YM for PCL, PCL/MgO (90/10), PCL/MgO (75/25) and PCL/MgO (50/50) was found to be 21.6, 24.8, 25.9 and 25.3 MPa respectively. Similarly, the YM for PCL/CS, PCLCS/MgO (90/10), PCL-CS/MgO (75/25) and PCL-CS/MgO (50/50) was found to be 6.8, 7.0, 7.5, and 8.6 MPa respectively. There was a significant difference ( $p = .03291$ ) in YM between samples PCL/MgO (90/10) and PCL. Furthermore, there was no significant difference in YM when the concentration of MgO was increased to 50%. There was a significant decrease in YM when CS was added to PCL. However, there was no significant difference in YM observed when different concentrations of MgO were added to PCL-CS.

### 3.3. X-ray diffraction crystallographic analysis

XRD patterns of as-spun PCL/MgO nanofibers with different ratios of PCL to MgO are shown in Fig. 6. The PCL nanofiber membrane showed two strong peaks at  $21.5^\circ$  and  $23.6^\circ$ , corresponding to the (1 1 0) and (2 0 0) crystallographic planes of PCL [18]. The chitosan peaks are found to overlap with the PCL peaks observed in this result.

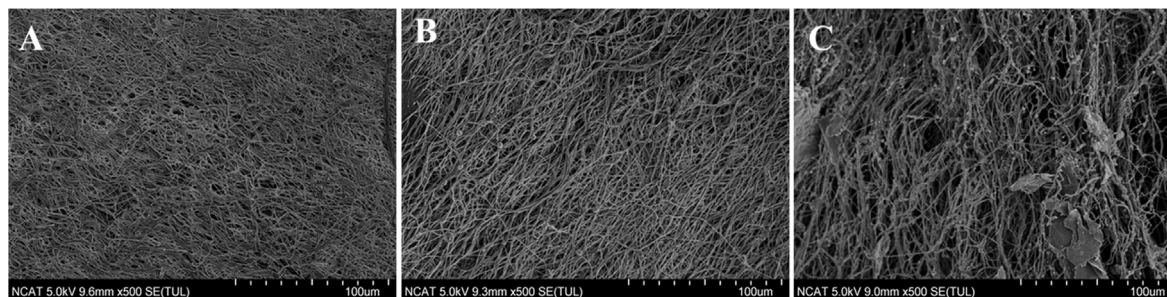


Fig. 3. Representative SEM images showing the morphology of nanofiber membranes after 3 weeks in 1X PBS. Images A, B and C represent PCL, PCL/CS and PCL-CS/MgO (50/50) respectively.

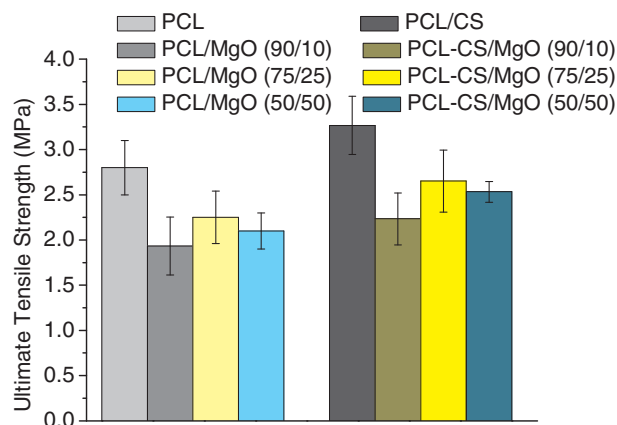


Fig. 4. Ultimate tensile strength of PCL, PCL/MgO and PCL-CS/MgO based nanofiber membranes,  $n = 3$ .

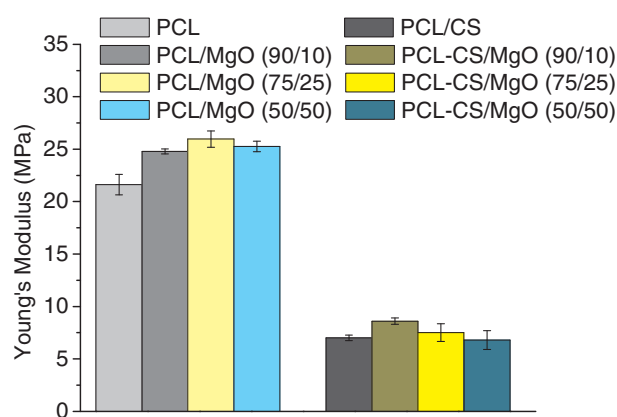


Fig. 5. Young's Modulus of PCL, PCL/MgO and PCL-CS/MgO based nanofiber membranes,  $n = 3$ .

Major MgO peaks were observed at  $38.9^\circ$ ,  $44.5^\circ$ ,  $63.25^\circ$  corresponding to (1 1 1), (2 0 0), and (2 2 0) crystallographic planes of MgO respectively [31]. These peaks were also observed in the PCL/MgO (50/50) fabric sample.

### 3.4. FTIR analysis

The FTIR spectra were measured to confirm the presence of PCL and CS of the composite nanofiber membrane. Fig. 7(A and B) shows the FTIR spectra of PCL and PCL-CS based nanofiber membranes respectively with different MgO content. Typical absorption bands for PCL nanofiber were located at:  $2950\text{ cm}^{-1}$  and  $2865\text{ cm}^{-1}$  for  $\text{CH}_2$  asymmetric and symmetric stretching vibrations respectively;  $1727\text{ cm}^{-1}$  for the stretch of CO in ester groups;  $1240\text{ cm}^{-1}$  and  $1170\text{ cm}^{-1}$  for C–O–C asymmetric and symmetric stretching vibrations, respectively

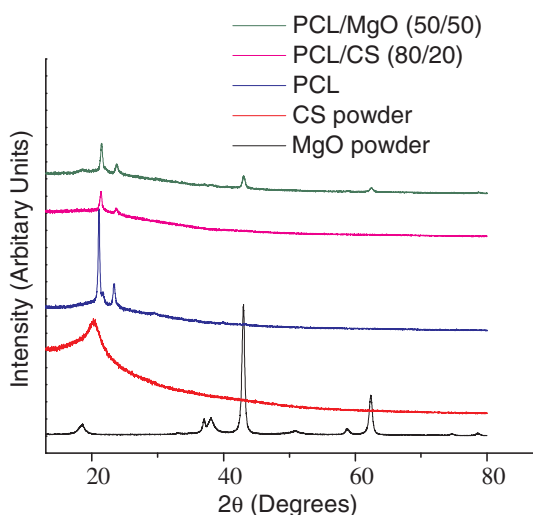


Fig. 6. X-ray diffraction patterns of PCL, PCL/CS, and PCL/MgO nanofibers membranes.

[32]. These peaks were also present in all other nanofiber membrane with CS and different MgO content. In chitosan based nanofiber, additional peaks were observed at  $1545\text{ cm}^{-1}$  and  $1630\text{ cm}^{-1}$  corresponding to amine and amide groups of chitosan.

### 3.5. pH change

Cell culture media were analyzed for pH change after days 1, 2, and 3 (See Figs. 8 and 9). The initial pH of media was 7.2. For day 1, average pH for PCL, PCL/MgO (90/10), PCL/MgO (75/25) and PCL/MgO (50/50) was found to be 7.35, 7.57, 7.91, 7.98 respectively. At Day 2, these values were found to be 7.42, 7.75, 8.07, 8.09 respectively. Similarly, at Day 3 these values changed to 7.39, 7.59, 7.95, 8.01 respectively.

Furthermore, at day 1 the average pH for PCL/CS, PCL-CS/MgO (90/10), PCL-CS/MgO (75/25) and PCL-CS/MgO (50/50) was found to be 7.62, 7.74, 8.16, 8.18, respectively. At day 2, these values were found to be 7.78, 7.86, 8.37, 8.39 respectively. Similarly, at day 3, these values changed to 7.66, 7.78, 8.20, 8.22 respectively.

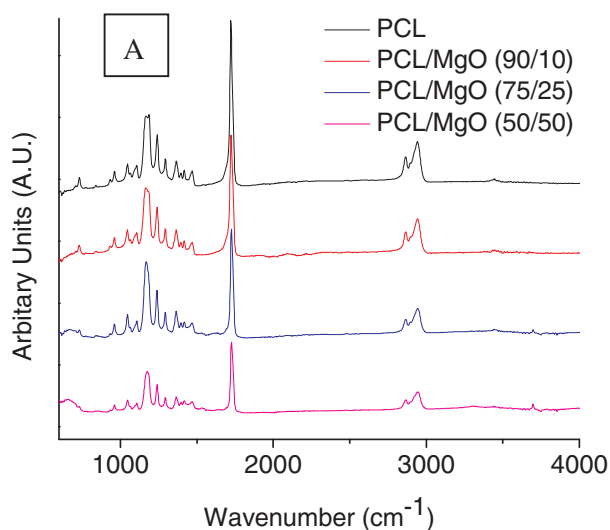


Fig. 7. FTIR spectra for PCL (A) and PCL-CS (B) based nanofibers membranes with different MgO content.

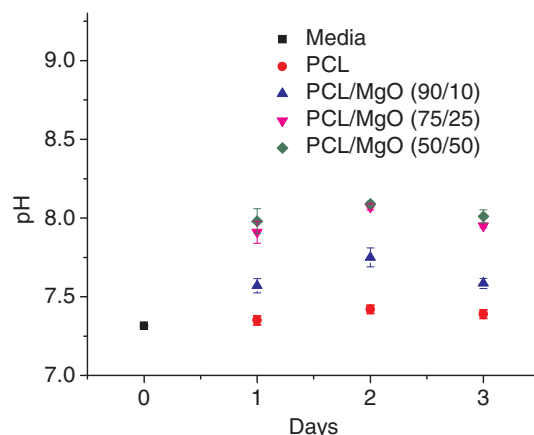


Fig. 8. pH change in cell culture media for PCL, and PCL/MgO based nanofiber membranes after days 1, 2, and 3.

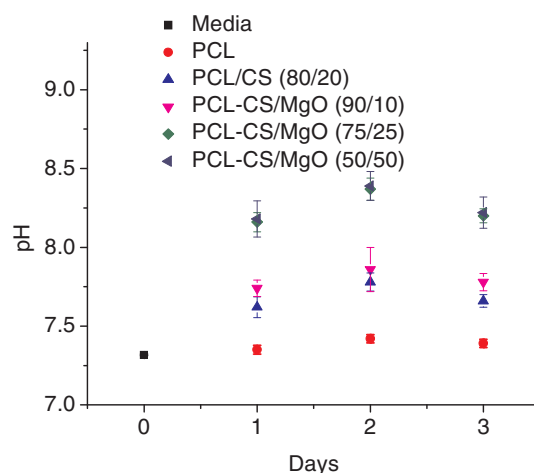


Fig. 9. pH change in cell culture media for PCL, and PCL-CS/MgO based nanofiber membranes after days 1, 2, and 3.

### 3.6. Cellular activity and Alamar Blue assay

Fig. 10 shows relative levels of AB between 3T3 cells grown on nanofiber membranes with and without MgO. Cytotoxicity was

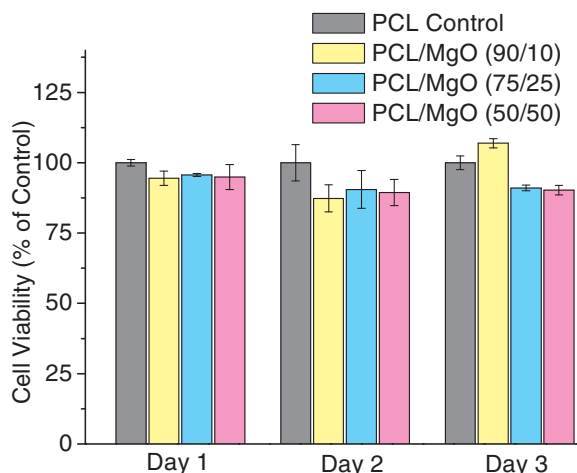


Fig. 10. Cytotoxicity result of 3T3 cells grown on PCL (control) and PCL/MgO based nanofiber membranes.

calculated for each time point using the control group (PCL) as a baseline for healthy cell culture as instructed in assay protocols. Toxicity level of 3T3 cells was similar to or slightly lower than the control groups. The average cell viability for PCL, PCL/MgO (90/10), PCL/MgO (75/25) and PCL/MgO (50/50) after day 1 was found to be 100%, 94.5%, 95.6% and 94.9% respectively. Similarly, after day 2, the average cell viability for these nanofiber was found to be 100%, 87.4%, 90.5% and 89.4% respectively. A significant difference ( $p = .04951$ ) was observed between samples PCL at day 1 and PCL/MgO (90/10) at day 2. Also, there was significant difference different ( $p = .04951$ ) between PCL/MgO (90/10) and PCL at day 2. Furthermore, after day 3, the average cell viability for PCL, PCL/MgO (90/10), PCL/MgO (75/25) and PCL/MgO (50/50) was found to be 100%, 106.9%, 91.0% and 90.2% respectively. Significant differences ( $p = .00302$ ;  $p = .00039$ ) were observed between samples PCL/MgO (75/25) and PCL, and PCL/MgO (75/25) and PCL/MgO (90/10) respectively at day 3. Significant difference ( $p = .00139$ ;  $p = .000211$ ) was also observed between samples PCL/MgO (50/50) and PCL, and PCL/MgO (50/50) and PCL/MgO (90/10) at day 3 respectively. There was a significant difference ( $p < .05$ ) between sample, PCL/MgO (90/10) from day 3, to samples PCL/MgO (90/10), PCL/MgO (75/25) and PCL/MgO (50/50) from day 2.

Furthermore, Fig. 11 shows average cell viability for samples consisting of chitosan and MgO. The average cell viability for PCL, PCL/CS, PCL-CS/MgO (90/10), PCL-CS/MgO (75/25) and PCL-CS/MgO (50/50) after day 1 was found to be 100%, 103.6%, 113.0%, 94.9% and 89.6%

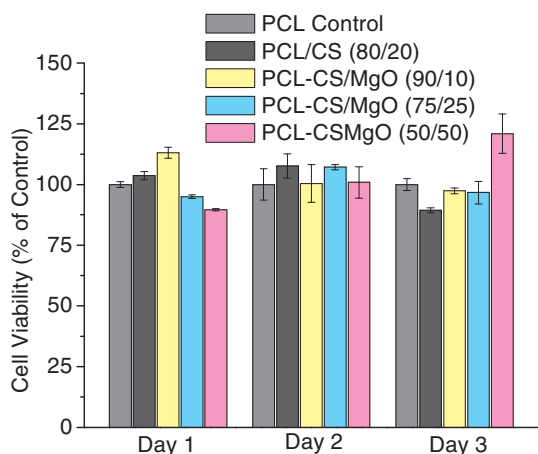


Fig. 11. Cytotoxicity result of 3T3 cells grown on PCL (control) and PCL-CS/MgO based nanofiber membranes.

respectively. PCL-CS/MgO (90/10) was significantly different ( $p = .0311$ ;  $p = .00134$ ;  $p = .00049$ ) to PCL, PCL-CS/MgO (75/25) and PCL-CS/MgO (50/50) at day 1 respectively. There was also a significant difference ( $p = .01764$ ) between samples PCL/CS and PCL-CS/MgO (50/50) at day 1.

Similarly, after day 2, the average cell viability for PCL, PCL/CS, PCL-CS/MgO (90/10), PCL-CS/MgO (75/25) and PCL-CS/MgO (50/50) was found to be 100%, 107.6%, 100.4%, 107.1% and 100.86% respectively. PCL/CS from day 2 was significantly different ( $p = .03963$ ;  $p = .00142$ ) with samples PCL-CS/MgO (75/25) and PCL-CS/MgO (50/50) from day 1, respectively. Furthermore, after day 3, the average cell viability for PCL, PCL/CS, PCL-CS/MgO (90/10), PCL-CS/MgO (75/25) and PCL-CS/MgO (50/50) was found to be 100%, 89.3%, 97.4%, 96.7% and 120.9%, respectively. PCL-CS/MgO (50/50) was significantly different ( $p < .05$ ) with all other samples at day 3. PCL-CS/MgO (50/50) from day 3 was also significantly different ( $p < .05$ ) to samples PCL, PCL/CS, PCL-CS/MgO (75/25) from day 1. PCL-CS/MgO (90/10) from day 1 was significantly different ( $p = .00318$ ) with PCL-CS/MgO (90/10) from day 3. PCL-CS/MgO (50/50) at day 3 was significantly different ( $p < .05$ ) with samples PCL, PCL-CS/MgO (90/10), PCL-CS/MgO (50/50) from day 2.

### 3.7. Cell attachment

Cellular compatibility including cell adhesion and spreading, as well as cell interactions with the nanofibrous membranes of the PCL, PCL/CS, PCL/MgO and PCL/CS-MgO, were studied by SEM. Fig. 12 shows the SEM images of fibroblast cells (3T3 cells) grown on these nanofibers after 3 days in cell culture. The cells attached well and formed cell clusters on the nanofibrous structure.

## 4. Discussion

In this research, composite nanofibers of PCL and PCL/chitosan with different compositions of MgO powders were obtained by electrospinning technique. Preparation of homogeneous solution with appropriate viscosity is an important step in electrospinning of nanofibers. In our experiment chitosan was added drop-wise to PCL/MgO solution to form a homogeneous blend solution that could be electrospun. In our own preliminary experiment, we prepared multiple ratios of PCL and chitosan, and found that any ratios with more than 40% of chitosan was not appropriate for electrospinning because the solution did not remain homogeneous for an extended duration (phase separation was visible after ~5 min). Therefore, we kept chitosan ratio constant, i.e. 20% of PCL solution, and varied the amount of MgO. PCL, being a nonionic synthetic polymer, is only soluble in organic solvent. TFE, an organic solvent, is a water-miscible fluorinated alcohol that has been widely used to dissolve PCL to create nanofibers. TFE exhibits a strong acidic nature due to the presence of electronegative trifluoro groups. TFE thus helps to create a stable interactions between MgO, CS and PCL by forming hydrogen bonding among them [26]. That may be one of the reason we could form a stable electrospinning solution with different compositions of PCL or PCL-CS and MgO.

All blended solutions in this study yielded nanofibers which were collected as a thin mat. However, fiber morphology slightly varied with blend composition. There is a significant difference in the fiber diameters between PCL fibers and corresponding fibers blended with MgO nanoparticles. This may be due to the presence of oxide particles enhancing the electrical conductivity of the solution, which further increases the acceleration of jetting during the electrospinning process [33]. Presence of soluble magnesium (i.e.  $Mg^{++}$ ) in the electrospun solution produced smaller diameter nanofibers. These nanofiber mats had good three-dimensional interconnected fibrous networks, with fiber diameters in the range of 0.7–1.3  $\mu m$ , which provided high surface area to volume ratio. High surface area with a nanopore structure serves as a better scaffold for cell attachment and ECM for cell growth.

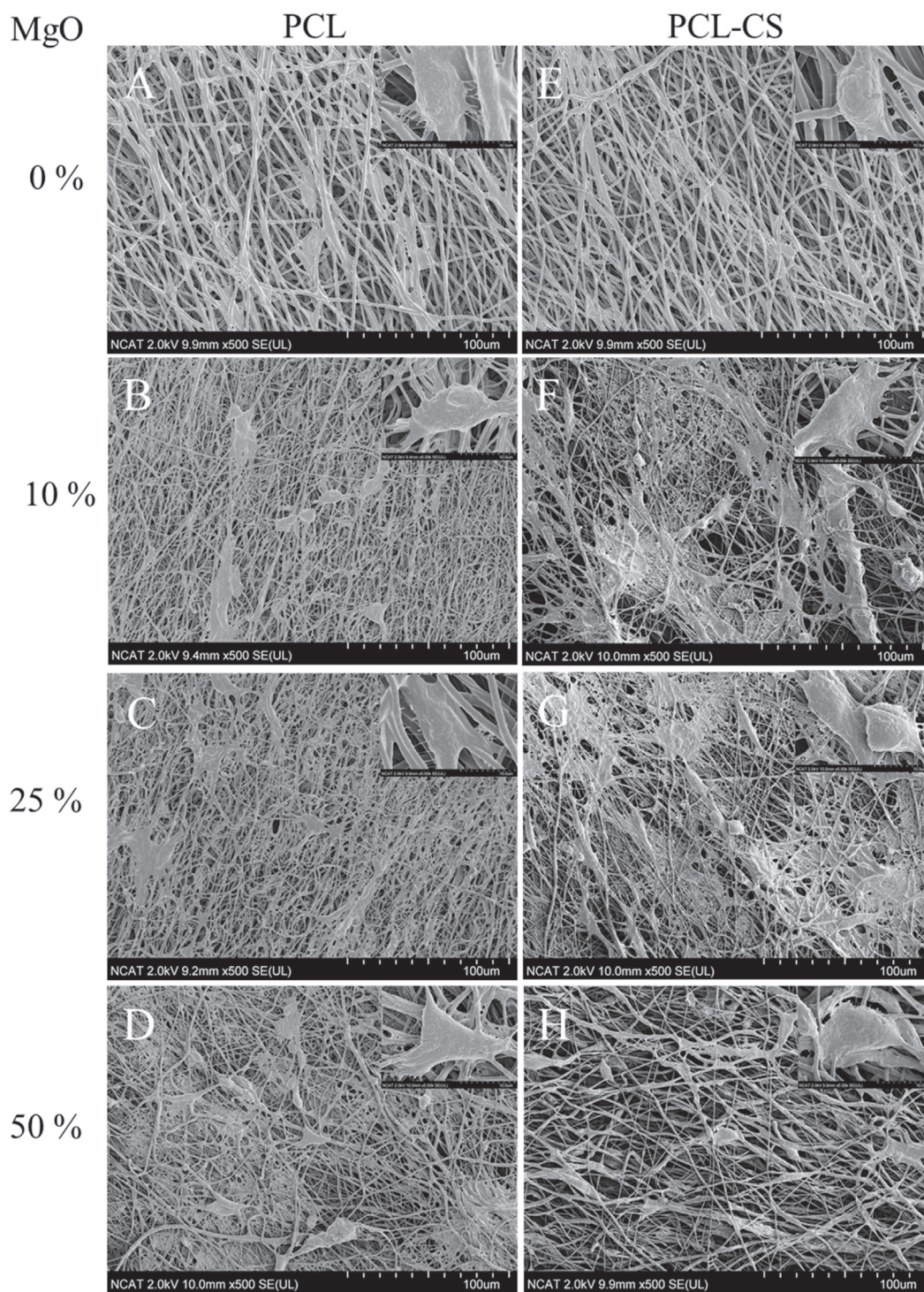


**Fig. 12.** SEM images showing the morphology of 3T3 fibroblast cells seeded on nanofiber membranes for 3 days. Images A to H represent PCL, PCL/MgO (90/10), PCL/MgO (75/25), PCL/MgO (50/50), PCL/CS, PCL-CS/MgO (90/10), PCL-CS/MgO (75/25) and PCL-CS/MgO (50/50) respectively. Insets are the higher magnification images of the corresponding SEM images of the nanofiber.

Nanofibers for tissue engineering require a highly porous and interconnected fibrous structure to ensure a biological environment conducive to cell attachment and proliferation as well as tissue growth and flow of nutrients [34,35].

Nanofiber membranes retained their dimensional stability and fibrous structure after immersion in PBS for up to 3 weeks. PCL is a known biopolymer with proven long biodegradation time of over 2 years. CS is a water soluble and relatively faster degradable polymer.

Our composite nanofiber consisted of only small amount of CS relative to PCL (~20% of PCL) which enabled the nanofiber membrane to be stable in aqueous medium. A prolonged immersion of the membrane in PBS for up to a year might be necessary to observe any drastic physical and chemical changes in fibers.

XRD patterns of as-spun PCL, PCL/CS, and PCL/MgO nanofibers showed that the highly crystalline nature of PCL was significantly weakened in the blended nanofibers. The lower crystallinity of PCL

indicates better miscibility of blended nanofibers [36]. This reduced crystallinity is likely to be due to the formation of lower degree of molecular order in the PCL/CS and PCL/MgO nanofibers primarily caused by close molecular interactions during the electrospinning process [18]. Characteristic FTIR absorption bands at  $1727\text{ cm}^{-1}$  and  $1545\text{ cm}^{-1}$  confirmed the presence of PCL and chitosan, respectively, as shown in Fig. 7. PCL/MgO and PCL-CS/MgO nanofibers showed the characteristic bands of PCL and CS. Absorption peaks of MgO are not clearly visible in composite nanofibers, because of their weak intensity compared to PCL and CS. Peak intensities of CS are also weak compared to PCL because of its small composition.

Nanofibrous scaffolds need to maintain their structural and mechanical integrity during *in vivo* and *in vitro* cell growth and tissue remodeling [18]. It is highly preferable to have the elastic modulus of the material to be close to that of target tissue to avoid any possible stress-shielding effects. The Young's Modulus (YM) and ultimate tensile strength (UTS) of PCL-MgO and PCL/CS-MgO were in the range of 6–21 MPa, and 1.9–3.3 MPa, respectively. The YM for polymeric nanofibers increased as we added inorganic MgO particles to the PCL solution. The presence of MgO particles resisted the elongation of nanofibers, resulting in increased YM. However, there was slight decrease in UTS. We believe that the decrease in UTS of the nanofibers with addition of MgO was due to the failure of nanofibers at interphase region of polymer and particle before reaching breaking point of polymer alone. Furthermore, the YM for nanofibers decreased while the UTS increased as we added chitosan to the PCL solution. However, this increase in UTS isn't statistically significant. This small increase of strength can be attributed to strong intermolecular hydrogen bonding interactions between PCL carbonyl groups and chitosan amine groups. On the other hand, YM of PCL-CS was significantly lower than PCL. Chitosan used in our experiment had very small molecular weight ( $\sim 2.5\text{ kDa}$ ) which might have negative impact on modulus of PCL fiber. Another factor which affects the modulus of membrane is the fiber orientation. Our SEM images showed better alignment in PCL fiber than in PCL-CS fiber. Previous studies have shown that randomly oriented fibers deform to a greater strain and have lower modulus than oriented fiber [37]. However, increased percentage of MgO in PCL-CS did not cause a significant difference in Young's Modulus. The strength of the nanofiber decreased after the introduction of MgO into the PCL-CS solution. There was no significant difference in the ultimate strength of the nanofibers that consisted different percentages of MgO. Despite some variation of modulus of these fibers with different compositions, their average YM values are comparable to the modulus of animal tissues i.e. human articular cartilage (1–10 MPa) [38,39], bovine articular cartilage (2–7 MPa) [39], liver and kidney (1–15 MPa) [40,41], artery and vein (0.6–3.5 MPa) [42].

Cell viability was assessed using an Alamar Blue (AB) assay. The dye, AB, is a chemical resazurin that enters the living cells and turns into pink fluorescent molecules due to the reduction of resazurin to resorufin with mitochondrial reductases [18,43]. The amount of dye consumed is proportional to cellular metabolic activity, which is proportional to cell number. A relative measure of cell numbers was obtained from the control. There have been several studies in the literatures that confirms the nontoxic nature of PCL to 3T3 fibroblasts as well as other cells [18,32]. Hence, we used our PCL sample as a positive control in this study. Cell cytotoxicity on the nanofiber were found to be non-significant ( $p > .05$ ) for days 1, 2 and 3, which substantiates that these scaffolds can provide adequate and non-toxic support for 3T3 cells to grow and proliferate. According to the current ISO standards (ISO 10993, part 5), cell viability higher than 75% could be considered as non-toxic for medical devices, so we defined the Mg ion concentration with 75% cell viability as the safety level in our experiment [44]. All of our fibers in this experiment showed cell viability greater than or equal to 75%.

The possible primary toxicants in these nanofibers could be the excessive leachants from the nanofibers – that includes released Mg

ions. Our cell toxicity results indicate that these fibers didn't release the Mg in sufficiently high level that could be toxic to the cells. In our previous study it was observed that there was very insignificant change of cumulative release of Mg ions from PCL-based fibers [26]. Recent research has shown that the safety level of Mg ion is 35 mM for L929 cells and osteoblast cells, and 15 mM for BMSCs and MC3T3-E1 [17,44].

MgO-based composite fibers when in contact with aqueous medium can form a soluble form of Mg, such as magnesium hydroxide. Formation of hydroxides could easily increase the pH of the medium. We measured the pH of the culture media obtained from the cell seeding experiments to find out if the increased pH of the culture media can be correlated with cell toxicity. pH of the media collected from the composite fibers increased compared to the pH of the culture media alone (Figs. 8 and 9). The change of pH for both PCL and PCL/CS nanofibers was lower than the corresponding fibers with MgO. The higher pH values measured in MgO-containing nanofibers is attributed to the release of basic hydroxyl groups in the culture media [45]. Our culture media was DMEM, which contains carbonate buffers that controls the change of pH due to elevated gaseous carbon dioxide level in the incubator. pH of the media is controlled by high  $\text{CO}_2$  levels in the incubator (5% or more).

Furthermore, SEM images showed that the fiber topography enhanced the cell attachment on the fibers. All the nanofibers samples showed attachment of cells to the surfaces by forming numerous and long filopodia. It is interesting to observe that the filopodia of the cells tend to attach and grow along the nanofibers direction whose diameter is comparable to that of the filopodia. Such cellular morphology is another indicative of a favorable interaction of fibroblasts with the nanofibers.

## 5. Conclusions

PCL-CS/MgO based nanofibers were successfully fabricated by the electrospinning technique. All the fiber composition showed uniform surface morphology, structural integrity, and suitable mechanical properties. PCL/MgO showed higher Young's modulus ( $\sim 25\text{ MPa}$ ) compared to other compositions, whereas the ultimate tensile strength was higher for PCL/CS nanofiber ( $\sim 3\text{ MPa}$ ). XRD confirmed the oxide state of MgO in the nanofiber sample. Alamar Blue Assay revealed no toxicity in these fibers. SEM imaging confirmed favorable cell adhesion and cell attachment on these nanofibers. Cell viability was found to be  $> 75\%$  for all sample types, which is considered a safe level. These nanofiber samples showed the attachment of cells to the surfaces by numerous and long filopodia. The significance of this work was to synthesize a novel biomaterial scaffold for use in tissue engineering applications such as wound healing, bone regeneration, drug delivery and regenerative medicine. Electrospun PCL-CS/MgO-based nanofibers are inexpensive and easy to synthesize, process and scale up. The ability to produce a novel material represents a significant advancement in development of composite materials with structural and material properties that will be beneficial for biomedical applications.

## Acknowledgments

The authors acknowledge the support of the National Science Foundation Engineering Research Center for Revolutionizing Metallic Biomaterials (EEC-0812348) and the NSF Nanotechnology Undergraduate Education Grant (EEC-1242139) at North Carolina A&T State University.

## Conflict of Interest

The authors declare no conflict of interest.

## References

- [1] N. Bhattarai, Electrospun chitosan-based nanofibers and their cellular compatibility, *Biomaterials* 256 (31) (2005) 6176–6184.
- [2] M.P. Prabhakaran, et al., Electrospun biocomposite nanofibrous scaffolds for neural tissue engineering, *Tissue Eng. Part A* 14 (11) (2008) 1787–1797.
- [3] T. Dvir, et al., Nanotechnological strategies for engineering complex tissues, *Nat. Nanotechnol.* 6 (1) (2011) 13–22.
- [4] R.J. Wade, et al., Protease-degradable electrospun fibrous hydrogels, *Nat. Commun.* (2015) 6.
- [5] V. Leung, F. Ko, Biomedical applications of nanofibers, *Polym. Adv. Technol.* 22 (3) (2010) 350–365.
- [6] J.D. Hartgerink, E. Beniash, S.I. Stupp, Peptide-amphiphile nanofibers: a versatile scaffold for the preparation of self-assembling materials, *Proc. Natl. Acad. Sci. U.S.A.* 99 (8) (2002) 5133–5138.
- [7] B. Dhandayuthapani, et al., Polymeric scaffolds in tissue engineering application: a review, *Int. J. Polym. Sci.* (2011).
- [8] K. Jayaraman, et al., Recent advances in polymer nanofibers, *J. Nanosci. Nanotechnol.* 4 (1–2) (2004) 52–65.
- [9] P.X. Ma, R.Y. Zhang, Synthetic nano-scale fibrous extracellular matrix, *J. Biomed. Mater. Res.* 46 (1) (1999) 60–72.
- [10] T.J. Sill, H.A. von Recum, Electrospinning: applications in drug delivery and tissue engineering, *Biomaterials* 29 (13) (2008) 1989–2006.
- [11] N. Bhattarai, et al., Natural-synthetic polyblend nanofibers for biomedical applications, *Adv. Mater.* 21 (27) (2009) 2792.
- [12] B. Feng, et al., Effect of inhomogeneity of the electrospun fibrous scaffolds of gelatin/polycaprolactone hybrid on cell proliferation, *J. Biomed. Mater. Res., Part A* 103 (2) (2015) 431–438.
- [13] H.Q. Cao, T. Liu, S.Y. Chew, The application of nanofibrous scaffolds in neural tissue engineering, *Adv. Drug Deliv. Rev.* 61 (12) (2009) 1055–1064.
- [14] A. Cooper, N. Bhattarai, M.Q. Zhang, Fabrication and cellular compatibility of aligned chitosan-PCL fibers for nerve tissue regeneration, *Carbohydr. Polym.* 85 (1) (2011) 149–156.
- [15] S.J. Ashleigh Cooper, N. Bhattarai, Miqin Zhang, Aligned chitosan-based nanofibers for enhanced myogenesis, *J. Mater. Chem.* 20 (40) (2010) 8904–8911.
- [16] S. Khanal, et al., pH-Responsive PLGA nanoparticle for controlled payload delivery of diclofenac sodium, *J. Funct. Biomater.* 7 (3) (2016).
- [17] U. Adhikari, et al., Magnesium incorporated chitosan based scaffolds for tissue engineering applications, *Bioact. Mater.* 1 (2) (2016) 132–139.
- [18] A. Edwards, D. Jarvis, T. Hopkins, S. Pixley, N. Bhattarai, Poly( $\epsilon$ -caprolactone)/keratin-based composite nanofibers for biomedical applications, *J. Biomed. Mater. Res. Part B* 103 (1) (2015) 21–30.
- [19] I. Slutsky, et al., Enhancement of learning and memory by elevating brain magnesium, *Neuron* 65 (2) (2010) 165–177.
- [20] C.S. Anast, et al., Evidence for parathyroid failure in magnesium deficiency, *Science* 177 (4049) (1972) 606–1000.
- [21] H. Zreiqat, et al., Mechanisms of magnesium-stimulated adhesion of osteoblastic cells to commonly used orthopaedic implants, *J. Biomed. Mater. Res.* 62 (2) (2002) 175–184.
- [22] H. Ebel, T. Gunther, Magnesium-Metabolism - a Review, *J. Clin. Chem. Clin. Biochem.* 18 (5) (1980) 257–270.
- [23] M.M. Fagian, L.P. Da Silva, A.E. Vercesi, Inhibition of oxidative phosphorylation by Ca<sup>2+</sup> or Sr<sup>2+</sup>: a competition with Mg<sup>2+</sup> for the formation of adenine nucleotide complexes, *Biochim. Biophys. Acta* 852 (2–3) (1986) 262–268.
- [24] L.A.D.G. Garfinkel, Magnesium regulation of the glycolytic pathway and the enzymes involved Magnesium, 4 (1985) (2–3), 60–72.
- [25] S. Sundarrajan, S. Ramakrishna, Fabrication of nanocomposite membranes from nanofibers and nanoparticles for protection against chemical warfare stimulants, *J. Mater. Sci.* 42 (20) (2007) 8400–8407.
- [26] M. Boakye, et al., Fabrication and characterization of electrospun PCL-MgO-keratin-based composite nanofibers for biomedical applications, *Materials* 8 (7) (2015) 4080.
- [27] S. Dadvar, H. Tavanai, M. Morshed, Fabrication of nanocomposite PAN nanofibers containing MgO and Al<sub>2</sub>O<sub>3</sub> nanoparticles, *Polym. Sci. Ser. A* 56 (3) (2014) 358–365.
- [28] S. Dadvar, H. Tavanai, M. Morshed, UV-protection properties of electrospun polyacrylonitrile nanofibrous mats embedded with MgO and Al<sub>2</sub>O<sub>3</sub> nanoparticles, *J. Nanopart. Res.* 13 (10) (2011) 5163–5169.
- [29] N.P. Rijal, U. Adhikari, N. Bhattarai, Magnesium Incorporated Polycaprolactone-Based Composite Nanofibers, in: *ASME 2015 International Mechanical Engineering Congress and Exposition, American Society of Mechanical Engineers*, 2015.
- [30] J. Gunn, M.Q. Zhang, Polyblend nanofibers for biomedical applications: perspectives and challenges, *Trends Biotechnol.* 28 (4) (2010) 189–197.
- [31] L.-X. Li, et al., Excellent fluoride removal properties of porous hollow MgO microspheres, *New J. Chem.* 38 (11) (2014) 5445–5452.
- [32] S.R. Gomes, et al., In vitro and in vivo evaluation of electrospun nanofibers of PCL, chitosan and gelatin: a comparative study, *Mater. Sci. Eng. C* 46 (2015) 348–358.
- [33] R. Nirmala, et al., Preparation and characterization of copper oxide particles incorporated polyurethane composite nanofibers by electrospinning, *Ceram. Int.* 39 (8) (2013) 9651–9658.
- [34] L.Y. Jiang, Y.B. Li, C.D. Xiong, Preparation and biological properties of a novel composite scaffold of nano-hydroxyapatite/chitosan/carboxymethyl cellulose for bone tissue engineering, *J. Biomed. Sci.* 16 (2009).
- [35] Z.S. Li, et al., Chitosan-alginate hybrid scaffolds for bone tissue engineering, *Biomaterials* 26 (18) (2005) 3919–3928.
- [36] Y. Nishio, R. Manley, Blends of cellulose with nylon 6 and poly ( $\epsilon$ -caprolactone) prepared by a solution-coagulation method, *Polym. Eng. Sci.* 30 (2) (1990) 71–82.
- [37] K. Mubyana, et al., The influence of specimen thickness and alignment on the material and failure properties of electrospun polycaprolactone nanofiber mats, *J. Biomed. Mater. Res. A* 104 (11) (2016) 2794–2800.
- [38] S.F. Yang, et al., The design of scaffolds for use in tissue engineering. Part 1. Traditional factors, *Tissue Eng.* 7 (6) (2001) 679–689.
- [39] D. Lacroix, P.J. Prendergast, A mechano-regulation model for tissue differentiation during fracture healing: analysis of gap size and loading, *J. Biomech.* 35 (9) (2002) 1163–1171.
- [40] L.A. Herbert, et al., Mechanical properties of the dog renal capsule, *J. Appl. Physiol.* 40 (2) (1976) 164–170.
- [41] M. Hollenstein, et al., Mechanical characterization of the liver capsule and parenchyma, *Biomed. Simul., Proc.* 4072 (2006) 150–158.
- [42] C.T. McKee, et al., Indentation versus tensile measurements of Young's modulus for soft biological tissues, *Tissue Eng. Part B* 17 (3) (2011) 155–164.
- [43] J. O'Brien, et al., Investigation of the Alamar Blue (resazurin) fluorescent dye for the assessment of mammalian cell cytotoxicity, *Eur. J. Biochem.* 267 (17) (2000) 5421–5426.
- [44] J. Wang, et al., Recommendation for modifying current cytotoxicity testing standards for biodegradable magnesium-based materials, *Acta Biomater.* 21 (2015) 237–249.
- [45] P. Jha, K. Singh, Effect of MgO on bioactivity, hardness, structural and optical properties of SiO<sub>2</sub>-K<sub>2</sub>O-CaO-MgO glasses, *Ceram. Int.* 42 (1) (2016) 436–444.